Adaptive neural network and extended state observer-based non-singular terminal sliding modetracking control for an underactuated USV with unknown uncertainties

Gong Xing Wu[a,*], Yi Ding[a], Tezdogan Tahsin[b], Incecik Atilla [c]

[a] *College of Ocean Science and Engineering, Shanghai Maritime University, Shanghai, 201306, China*

[b] *Department of Civil, Maritime and Environmental Engineering, University of Southampton, UK*

[c] *Department of Naval Architecture, Ocean and Marine Engineering, University of Strathclyde, Glasgow, UK*

ABSTRACT

In this paper, a non-singular terminal sliding mode control (NTSMC) scheme based on adaptive neural network(NN) and nonlinear extended state observer (ESO) is proposed for trajectory tracking control of the underactuated unmanned surface vehicle (USV) in the presence of model uncertainties and external disturbances. Firstly, a three-degree-of-freedom USV nonlinear mathematical model is established,then a nonlinear ESO is constructed to estimate the unmeasurable velocities and lumped disturbances.Besides, a neural shunt model is introduced to eliminate the repetitive derivative of the virtual control law and reduce the difficulty of the control law design. On the basis of these and considering the USV position and speed errors, a non-singular terminal sliding surface is constructed to achieve fast convergence.Meanwhile, the minimum learning parameter (MLP) neural network algorithm is designed to estimate the model uncertainties.Subsequently, an adaptive law is designed to compensate for the NNapproximation errors and disturbances, which reduces the computational burden and enhances the robustness of the system. Finally, by using Lyapunov theory, it is proved that the designed control law can guarantee the uniform boundedness of all error signals in the closed-loop system.Comparative simulation results further confirm the effectiveness and superiority of the proposed method.

Keywords: Underactuated unmanned surface vehicle; Trajectory tracking control; Extended state observer; Neural shunt model; Nonsingular terminal sliding mode; Minimum learning parameter

1. Introduction

Unmanned surface vehicle (USV) is a typeof unmanned surface platform with autonomous navigation capability, which can perform some specified tasks in complex

*E-mail: wugx@shmtu.edu.cn.

This is a peer reviewed, accepted author manuscript of the following research article: Wu, G. X., Ding, Y., Tahsin, T., & Atilla, I. (2023). Adaptive neural network and extended state observer-based non-singular terminal sliding modetracking control for an underactuated USV with unknown uncertainties. *Applied Ocean Research*, 135, [103560]. https://doi.org/10.1016/j.apor.2023.103560

marine environments by carrying different modern intelligent equipment(Mu et al., 2017). Due to the advantages of small volume, fast speed, low cost, strong maneuverability, and no casualties(Chen et al., 2018; Liu et al., 2016), USV possessesextensive application prospects in the military and civilian fields,such as surveillance, reconnaissance and anti-submarine(Lin et al., 2022), searchand disaster rescue(Zhou et al., 2020),environmental monitoring and water sampling(Jiang et al., 2019),etc.However, in the real marine environment, USV is inevitably vulnerable to complex disturbances caused by external winds, waves and ocean currents, soits nonlinear, time delay and model uncertainties make the design of USV control system more complex and challenging(Yao, 2022). This topic has therefore become a hot research topic recently attracting extensive interest from researchers worldwide.

Trajectory tracking control of underactuated ships is an important topic in the field of ship control. Many researchers have made significant outstanding contributions and proposed many nonlinear control methods, such as backstepping control(Piao et al., 2020), sliding mode control(Chen et al., 2022), event-triggered control(Deng et al., 2020), robust fault–tolerant control(Qin et al., 2019), model predictive control (Martinsen et al., 2022), and the combination of various control methods.(Zhao et al., 2021)designed a tracking controller by combining backstepping and adaptive sliding mode control technology, and guaranteed the control system error is ultimately uniformly bounded through Lyapunovstability theoretical analysis. However, the backstepping method requires the calculationof the duplicate derivatives of virtual control variables in the design process,which is not conducive to controller design(Zhang et al., 2022).(Zhang et al., 2020) proposed a robust controller by employing a second-order filter to acquire the derivation of virtualvariables, it effectively reduces the computational complexities of the traditional backstepping method.However, the above-mentioned controllers are not well considered the influence of model uncertainties and external disturbances, which do not conform to practical ship control engineering. Therefore, achieving an accurate trajectory tracking control is still a challenge for ship control.

In the practical ocean environment, ships are vulnerable to some unknown disturbances and uncertainties, and their model parameters will also change (Mu et al., 2018), which will significantly reduce the tracking performance and even lead to mission failure. To overcomethese challenges, the sliding mode controller has strong robustness and has significant advantages in resisting external disturbances and model parameter changes(Wan et al., 2018).In (Chen et al., 2022), a novel fixed-time fractional-order sliding mode control strategy was proposed forthe trajectory tracking of the USV, which realized the optimization of the sliding mode control. In (Sun et al., 2022), a compensation control algorithm based on a disturbance observer was proposed to eliminate external environmental disturbances. To address the influence of modeling uncertainties and external disturbances on ship systems, (Chen et al., 2020) used the universal approximation property of RBF neural network to approximate and compensate forthe modeling uncertainties.Meanwhile, the disturbance observer was employed to estimate external unknown disturbances,finally, the global stability of the global closed-loop system was verified by theoretical analysis.However, the RBF neural network algorithm requires online adjust all weight vectors of the network, which

increases the computational burden(Shen et al., 2020a).In light of that, it can be effectively solved by using the minimum learning parameter (MLP) method.In (Jiang et al., 2021), an adaptive algorithm was designed by combining the dynamic surface control (DSC) and the MLP-based NN technique,with only two online parameters being tuned to tackle the uncertainties, which reduces the computational load.

Although the control method mentioned above has a good control effect, the convergence speed is slow, and the chattering effect exists in the traditional sliding mode control(Rangel et al., 2020). The terminal sliding mode(TSM) is designed to solve this problem due to its excellent convergence speed, high precision, and strong robustness(Shen et al., 2020b).To avoid singularity in terminal sliding mode control law design, a robust controller based on an adaptive integral terminal sliding mode(AITSM) was designed by(Gonzalez-Garcia and Castaeda, 2021), which guaranteed finitetime state convergence and enhanced robustness.In the presence of complex unknowns including unmodeled dynamics and external environment disturbances, (Wang et al., 2021)designed a non-singular fast terminal sliding mode (NFTSM) control scheme and combined the finite time extended observer to estimate the lumped uncertainties.Finally, fast convergence and accurate trajectory tracking performance were achieved within a finite time.

Despite the existence of extensive research on ship track tracking, the main problem of the aforementioned studies is that very few consider actuator saturation. In practical application, input saturation inevitably exists due to the physical constraints of the propulsion system, which may lead to system instability if input saturation is ignored(Zhu and Du, 2020).In light of that, (Shen et al., 2022)adopted dynamic surface technology and introduced an auxiliary dynamic system (ADS) to avoid input saturation caused by the intermediate control law.Considering the velocity of practical marine vessels during navigation is unmeasurable, (Zhang et al., 2019)developed a fixed-time extended state observer (FXESO) to estimate the unmeasured velocities and lumped disturbances, and their estimation errors converge to the origin in fixed time.

In this paper, inspired by the above research,an NTSMC schemehas been proposedfor trajectory tracking of the underactuated USVbased on the nonlinear mathematical model with input saturation,model uncertainties, and external disturbances.This scheme combines a nonlinear ESO, neural shunt model, and MLP neural network with adaptive technology.The overall stability of the closed-loop control system is proved by Lyapunov theory and the tracking error variables can achieve fast convergence, the simulation results demonstrate the effectiveness and superiority of the proposed scheme. The main contributions of this paper aresummarized as follows:

(1) A non-singular terminal sliding mode surface is designed to achieve fast convergence, in which the hyperbolic tangent function is adopted instead of the original symbolic function to eliminate the actuator consumption caused by the "chattering" effect.
(2) A neural shunt model is introduced to solve the problem of "differential explosion" when designing the virtual control law, which reduces the difficulty of the control law design. Meanwhile, the MLP-based RBFNN and the adaptive technology are employed to deal with the model uncertainties and unknown disturbance bounds.

(3) A nonlinear ESO is developed to observe the unavailable USV velocitiesand estimates the lumped disturbances consisting of internal model uncertainties and external environmental disturbances.

The remaining of this paper is organized as follows.Section 2 introduces problem formulation and preliminaries. The design and stability analysis of the proposed NTSMC scheme and the ESO arepresented in Section 3.The numerical simulations and the comparison of the results arediscussed in Section 4.Finally,Section 5 summarizes this paper and describes future research.

2. Problem formulation and preliminary considerations

Throughout this paper, we adopt the followingnotations. $\Re \geq 0$ denotes the set of all nonnegative real numbers,and $\Re^n$ denotes the Euclidean space with dimension n. $|\square|$ represents the absolute value of a scalar. $\|\square\|$ denotes the Euclidean norm of a vector or the 2-norm of a matrix. $[\square]^T$ denotes thetranspose of a matrix $[\square]$,and $\mathrm{diag}(x_1, x_2, x_3) \in \Re^{3\times 3}$ be the diagonal matrix in which the diagonal elements are x_1 , x_2 , x_3 . $\lambda_{\min}(\square)$ is defined as the minimum eigenvalue of a matrix $(\square)$ .Besides,we define $sig^{\alpha}(x) = sign(x)|x|^{\alpha}$, $x \in \Re$, $\alpha \in (0,1)$,where $sign(\square)$ is a signum function.

2.1 Preliminary considerations

Before proceeding,we introduce some useful definitionsandlemmas.

Definition 1. For any $x \in \Re$, the hyperbolic tangent functionis defined as:

$$\tanh(x) = \frac{e^{x} - e^{-x}}{e^{x} + e^{-x}} \tag{1}$$

Lemma 1(Qiu et al., 2019).For any $\varepsilon > 0$ and $\zeta \in \Re$, the following inequality holds:

$$0 \leq |\zeta| - \zeta \tanh(\zeta / \varepsilon) \leq \kappa\varepsilon \tag{2}$$

where $\kappa = 0.2785$ satisfies $\kappa = e^{-(\kappa+1)}$.

Lemma 2(Lu et al., 2018)**.**Consider a nonlinearsystem $\dot{\boldsymbol{x}} = f(\boldsymbol{x}(t))$, $\boldsymbol{x} \in \Re$, if there exists a continuous and positive definite Lyapunov function $V(\boldsymbol{x})$ satisfying $k_1(\|\boldsymbol{x}\|) \leq V(\boldsymbol{x}) \leq k_2(\|\boldsymbol{x}\|)$ such that $\dot{V} \leq -lV + Q$, where k_1, k_2 are class κ functions and l , Q are positive constants, then thesolution $\boldsymbol{x}(t)$ is ultimately uniformly bounded(UUB).

Lemma 3(Zheng and Zou, 2016). For a given unknown continuous function $f(\boldsymbol{x})$: $\Re^m \to \Re$, it can be approximated over a compact set $\boldsymbol{\Omega}_x \subset \Re^m$ with the following RBFNN:

$$f(\boldsymbol{x}) = \boldsymbol{W}^{*T}\boldsymbol{h}(\boldsymbol{x}) + \varsigma_n \tag{3}$$

where $\boldsymbol{x} = [x_1, x_2, \cdots, x_m]^T \in \Re^m$ is the input vector, $\boldsymbol{W}^* = [W_1, W_2, \cdots, W_l]^T \in \Re^l$ represents the ideal weight vector, and l is the node number

ofRBFNN. $\boldsymbol{h}(\boldsymbol{x})=\left[h_1(x),h_2(x),\cdots,h_l(x)\right]^T\in\Re^l$ is a vector of RBF basis functions withthe form of Gaussian functions(4). ς_n is theapproximation error that is bounded over the compact set $\boldsymbol{\Omega}_x$, namely, $|\varsigma_n|\le\bar{\varsigma}_n$, where $\bar{\varsigma}$ is an unknown constant.

$$\boldsymbol{h}_i(\boldsymbol{x})=\exp\left(-\left\|\boldsymbol{x}-\boldsymbol{c}_i\right\|^2/2b_i^2\right),\quad i=1,2,\cdots,l \tag{4}$$

where $\boldsymbol{c}_i=\left[c_{i1},c_{i2},\cdots,c_{im}\right]^T\in\Re^m$ is the center of the receptive field and b_i is the width of the Gaussian function.

2.2USV mathematical model

In this section, we describe in detail the three-degree-of-freedom kinematics and dynamics of the underactuated USV in the presence of model uncertainties and external disturbances.

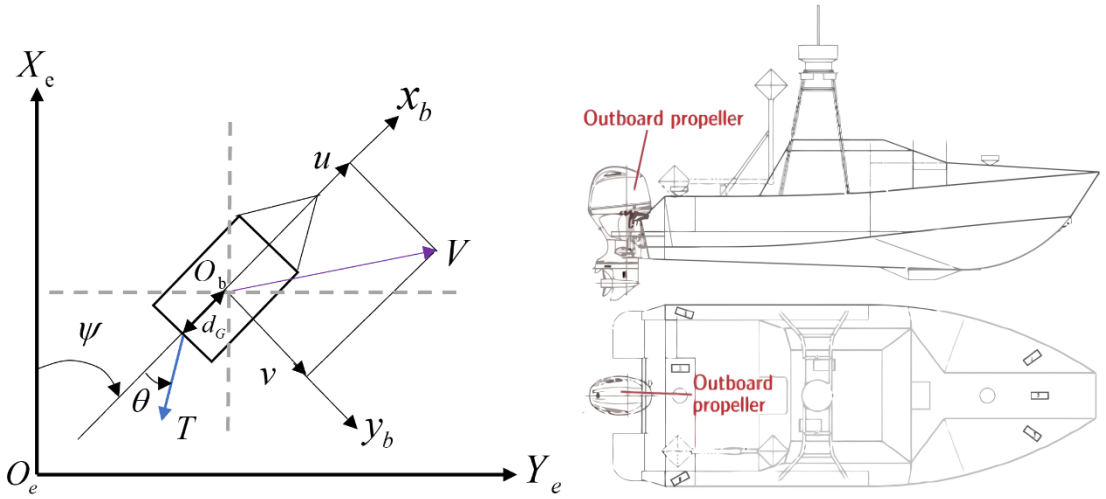

(a)The definition of two coordinate frames. (b) The schematic diagram ofthe outboard propeller.

Fig. 1. The schematic diagram of the USV planar motionand the outboard propeller for the USV.

As shown in Fig. 1(a),two coordinate framesare introduced to describe the USV motion in planar space, where $O_eX_eY_e$ is the earth-fixed frame and $o_bx_by_b$ the body-fixed frame.Referring to (Yu et al., 2019),the kinematics and dynamics mathematical model of the underactuated USV in horizontal motion can be established as:

$$\begin{cases}\dot{\boldsymbol{\eta}}=\boldsymbol{R}(\psi)\boldsymbol{\upsilon}\\ \boldsymbol{M}\dot{\boldsymbol{\upsilon}}+\boldsymbol{C}(\boldsymbol{\upsilon})\boldsymbol{\upsilon}+\boldsymbol{D}\boldsymbol{\upsilon}=\boldsymbol{\tau}+\boldsymbol{\tau}_d-\Delta\boldsymbol{f}\end{cases} \tag{5}$$

where $\boldsymbol{\eta}=[x,y,\psi]^T$ denotes the position (x,y) and the yaw angle ψ of the USV.The vector $\boldsymbol{\upsilon}=[u,v,r]^T$ describes the surge velocity$u$,the sway velocity v, and the yaw rate $r$of the USV. $\boldsymbol{R}(\psi)$ denotes the rotation matrix between body-fixed and inertia frame,which is definedas:

$$\boldsymbol{R}(\psi)=\begin{bmatrix}\cos\psi & -\sin\psi & 0\\ \sin\psi & \cos\psi & 0\\ 0 & 0 & 1\end{bmatrix} \tag{6}$$

withsatisfies $\boldsymbol{R}^{-1}(\psi)=\boldsymbol{R}^{T}(\psi)$ and $\|\boldsymbol{R}(\psi)\|=1$. $\boldsymbol{M}\in\Re^{3\times3}$ represents the positive definite inertia matrix including the USV mass and the hydrodynamic inertia; $\boldsymbol{C}(\boldsymbol{v})\in\Re^{3\times3}$ is the Coriolis and centripetal matrix; $\boldsymbol{D}\in\Re^{3\times3}$ is the damping matrix. $\boldsymbol{\tau}=[\tau_u,\tau_v,\tau_r]^T$ is the control input vector of the USV; $\boldsymbol{\tau}_d=[\tau_{du},\tau_{dv},\tau_{dr}]^T$ represents the unknown boundedexternal disturbances caused by winds, waves, and ocean currents.The vector $\Delta\boldsymbol{f}=\left[\Delta f_{\mathrm{u}},\Delta f_{\mathrm{v}},\Delta f_r\right]^T$ represents the unmodeled dynamics.The matrices $\boldsymbol{M}$, $\boldsymbol{C}(\boldsymbol{v})$ and $\boldsymbol{D}$ can be described as follows:

$$\boldsymbol{M}=\begin{bmatrix}m_{11} & 0 & 0\\ 0 & m_{22} & m_{23}\\ 0 & m_{32} & m_{33}\end{bmatrix},\boldsymbol{C}(\boldsymbol{v})=\begin{bmatrix}0 & 0 & a_{13}\\ 0 & 0 & a_{23}\\ a_{31} & a_{32} & 0\end{bmatrix},\boldsymbol{D}=\begin{bmatrix}d_{11} & 0 & 0\\ 0 & d_{22} & d_{23}\\ 0 & d_{32} & d_{33}\end{bmatrix} \tag{7}$$

where m_{11}, m_{22}, m_{33}, m_{23} and m_{32} denote the USV inertiamass and added mass;the terms d_{11}, d_{22}, d_{33}, d_{23} and d_{32} denote the hydrodynamic damping coefficients. In addition, $a_{13}=-a_{31}=-m_{22}v-m_{23}r$ and $a_{23}=-a_{32}=m_{11}u$ denote the Coriolis–centripetal terms.Referring to(Sun et al., 2019),the driving force and torque generated bytheoutboard propeller can be expressed as:

$$\boldsymbol{\tau}=\begin{bmatrix}\tau_u\\ \tau_v\\ \tau_r\end{bmatrix}=\begin{bmatrix}T\cos(\theta)\\ -T\sin(\theta)\\ d_G T\sin(\theta)\end{bmatrix} \tag{8}$$

where T represents the driving force produced by the propulsion system, θ represents the angle of the propulsion, and d_G represents the installed position of theoutboard propeller(see Fig. 1(b), it has a propulsionangle range given by $\theta\in[-30^{\circ},+30^{\circ}]$).

Remark 1. The USV is underactuated, which only generates surge force and yaw moment through theoutboard propeller, and no lateral propeller is directly used for control. In addition, if the steering angle of the outboard propeller θ is small, then itcan be assumed that $\tau_v\approx0$, and then $\boldsymbol{\tau}=[\tau_u,0,\tau_r]^T$.

Assumption 1. The USV is symmetrical and evenly distributed in mass, the barycenter of the USV coincides with the center of the body-fixed frame.Therefore, ignoring rolling, pitching, and heaving movements, and only considering the USV's three degrees-of-freedom motion insurging,swaying, and yawing.Sothe matrices $\boldsymbol{M}$ and $\boldsymbol{D}$ can be simplifiedas: $\boldsymbol{M}=diag(m_{11},m_{22},m_{33})$, $\boldsymbol{D}=diag(d_{11},d_{22},d_{33})$, $\boldsymbol{C}(\boldsymbol{v})$ can be written as:

$$\boldsymbol{C}(\boldsymbol{v})=\begin{bmatrix}0 & 0 & -m_{22}v\\ 0 & 0 & m_{11}u\\ m_{22}v & -m_{11}u & 0\end{bmatrix} \tag{9}$$

Therefore, the Equation (5)can be rewritten as the following state-space equations.

$$\begin{cases} \dot{x} = u\cos\psi - v\sin\psi \\ \dot{y} = u\sin\psi + v\cos\psi \\ \dot{\psi} = r \\ \dot{u} = \dfrac{1}{m_{11}}\left(m_{22}vr - d_{11}u + \Delta f_{\mathrm{u}}\right) + \dfrac{\tau_{\mathrm{u}} + \tau_{\mathrm{du}}}{m_{11}} \\ \dot{v} = \dfrac{1}{m_{22}}\left(-m_{11}ur - d_{22}v + \Delta f_{\mathrm{v}}\right) + \dfrac{\tau_{\mathrm{dv}}}{m_{22}} \\ \dot{r} = \dfrac{1}{m_{33}}\left[\left(m_{11} - m_{22}\right)uv - d_{33}r + \Delta f_{\mathrm{r}}\right] + \dfrac{\tau_{\mathrm{r}} + \tau_{\mathrm{dr}}}{m_{33}} \end{cases} \tag{10}$$

Moreover, due to the physical limit of the USV's propulsion system,the command control input signal calculated by the control law is inevitably subject to input saturation,which can be expressed as follows:

$$\tau_i = \begin{cases} sign(\tau_{ci})\tau_{i\max}, & |\tau_{ci}| > \tau_{i\max} \\ \tau_{ci}, & |\tau_{ci}| \le \tau_{i\max} \end{cases}, \quad i = u, r \tag{11}$$

where $\tau_i (i = u, r)$ are the actual control inputs; $\tau_{i\max} (i = u, r)$ denote the maximum control force or moment.

Assumption 2. In most working conditions,external disturbances $\tau_{di} (i = u, v, r)$ acting on the underactuated USV are generally considered to be superimposed by the unknown time-varying low-frequency periodic signals(Chen et al., 2019), which satisfy $|\tau_{di}| \le \tau_{di}^{\max}$, where $\tau_{di}^{\max} (i = u, v, r)$ are unknown positive constants.

Assumption 3. The desired trajectory (x_d, y_d) is sufficiently smooth and hasboundedfirst and second derivatives. In addition, the velocity vector $\boldsymbol{v} = [u, v, r]^T$ is unavailable.

3. Controller design and stability analysis

In this section, anadaptivenon-singular terminal sliding mode controller based on MLP and ESOis designed for tracking the trajectory of the underactuated USVwith unmodeled dynamics and external unknown time-varying ocean disturbances.For better illustration, the structural block diagram of the proposed trajectory tracking control scheme is shown in Fig. 2.

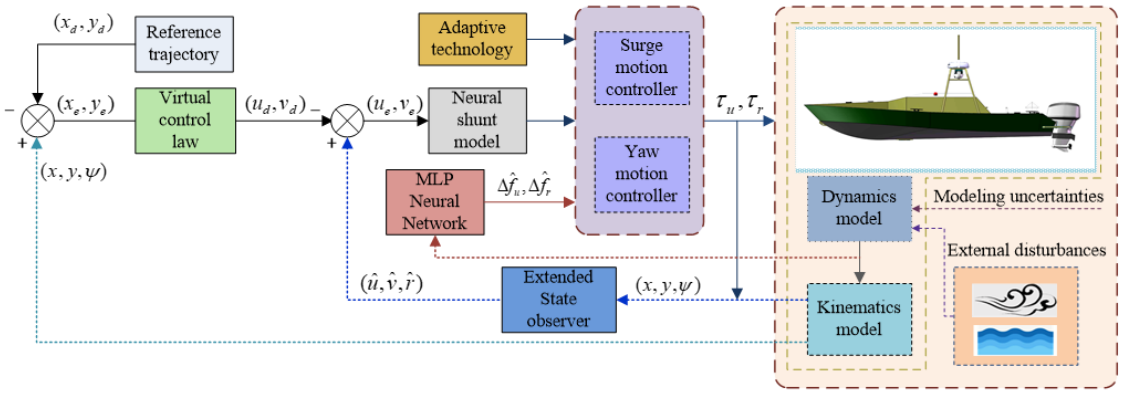

Fig. 2. The structural block diagram of the proposed trajectory tracking control scheme of the underactuated USV.

Thevirtual control law is designed to convert the desired position into the virtual state quantities, and the neural shunt model is introduced to handle the "explosion of complexity" problem caused by the differentiation of virtual control quantities.Moreover, the ESO is designed to obtain the exact estimations for the velocities and the lumped disturbances.Meanwhile,to enhance the robustness of the system,the MLP algorithm is adopted for approximating and compensating for the model uncertainties, which will reduce the computational complexity to some extent, and the adaptive technology is employed to estimate the neural network approximation error and the boundary value ofunknownexternaldisturbances.

The control objective of this paper is to design an NTSM trajectory tracking controller for the underactuated USV in the presence of model uncertainties, unmeasurable velocities, and unknown external ocean disturbances.Finally, the designed controllercould force the USVto navigatealong the desired trajectory (x_d, y_d) and ensure that all the tracking error signals of the closed-loop system converge on a small residual region and are uniformly bounded.

3.1 Design of nonlinear extended state observer

In this subsection,the ESO is designed to obtain the exact estimations for the velocities and the lumped disturbances. From USV mathematical model(5), the composite dynamics model of the systemcan be rewritten as:

$$\begin{aligned}\ddot{\boldsymbol{\eta}} &= \boldsymbol{R}(\psi)\dot{\boldsymbol{v}}+\dot{\boldsymbol{R}}(\psi)\boldsymbol{v} \\ &=\boldsymbol{R}(\psi)\boldsymbol{M}^{-1}\left[-\boldsymbol{C}(\boldsymbol{v})-\boldsymbol{D}\boldsymbol{v}+\boldsymbol{\tau}_d-\Delta\boldsymbol{f}\right]+\dot{\boldsymbol{R}}(\psi)\boldsymbol{v}+\boldsymbol{R}(\psi)\boldsymbol{M}^{-1}\boldsymbol{\tau} \\ &=\boldsymbol{\chi}+\boldsymbol{R}(\psi)\boldsymbol{M}^{-1}\boldsymbol{\tau}\end{aligned} \tag{12}$$

we let $\boldsymbol{x}_1=\boldsymbol{\eta}$, $\boldsymbol{x}_2=\dot{\boldsymbol{\eta}}$, then the dynamics model of the underactuated USV can be described as:

$$\begin{cases} \dot{\boldsymbol{x}}_1 = \boldsymbol{x}_2 \\ \dot{\boldsymbol{x}}_2 = \boldsymbol{\chi} + \boldsymbol{R}(\psi)\boldsymbol{M}^{-1}\boldsymbol{\tau} \end{cases} \tag{13}$$

where $\boldsymbol{\chi} = \boldsymbol{R}(\psi)\boldsymbol{M}^{-1}\left[-\boldsymbol{C}(\boldsymbol{v}) - \boldsymbol{D}\boldsymbol{v} + \boldsymbol{\tau}_d - \Delta\boldsymbol{f}\right] + \dot{\boldsymbol{R}}(\psi)\boldsymbol{v}$ represents the lumped uncertainty consisting of unmodeled dynamics and external disturbances.

Assumption 4(Van, 2019; Zhang et al., 2019)**.**The lumped uncertainty $\boldsymbol{\chi}$ satisfies $\|\dot{\boldsymbol{\chi}}\| \le H$, where $H > 0$ isan unknown bounded constant.

From (13), the nonlinear ESO can be constructed as follows

$$\begin{cases} \dot{\hat{\boldsymbol{x}}}_1 = \hat{\boldsymbol{x}}_2 + \dfrac{a_1}{\omega}(\boldsymbol{x}_1 - \hat{\boldsymbol{x}}_1) \\ \dot{\hat{\boldsymbol{x}}}_2 = \hat{\boldsymbol{\chi}} + \dfrac{a_2}{\omega^2}(\boldsymbol{x}_1 - \hat{\boldsymbol{x}}_1) + \boldsymbol{R}(\psi)\boldsymbol{M}^{-1}\boldsymbol{\tau} \\ \dot{\hat{\boldsymbol{\chi}}} = \dfrac{a_3}{\omega^3}(\boldsymbol{x}_1 - \hat{\boldsymbol{x}}_1) \end{cases} \tag{14}$$

where $\hat{\boldsymbol{x}}_1$, $\hat{\boldsymbol{x}}_2$ and $\hat{\boldsymbol{\chi}}$ are the estimates of $\boldsymbol{x}_1$, $\boldsymbol{x}_2$, and $\boldsymbol{\chi}$, respectively. ω and $a_i (i = 1,2,3)$ are positive design constants.

We define the observation error $\boldsymbol{E} = \left[\boldsymbol{e}_1, \boldsymbol{e}_2, \boldsymbol{e}_3\right]^T$, where $\boldsymbol{e}_1 = (\boldsymbol{x}_1 - \hat{\boldsymbol{x}}_1)/\omega^2$, $\boldsymbol{e}_2 = (\boldsymbol{x}_2 - \hat{\boldsymbol{x}}_2)/\omega$ and $\boldsymbol{e}_3 = \boldsymbol{\chi} - \hat{\boldsymbol{\chi}}$. By combining (14)we can obtain the following error equations.

$$\begin{cases} \omega\dot{\boldsymbol{e}}_1 = \dfrac{\dot{\boldsymbol{x}}_1 - \dot{\hat{\boldsymbol{x}}}_1}{\omega} = -\dfrac{a_1}{\omega^2}\left(\boldsymbol{x}_1 - \hat{\boldsymbol{x}}_1\right) + \dfrac{\boldsymbol{x}_2 - \hat{\boldsymbol{x}}_2}{\omega} = -a_1\boldsymbol{e}_1 + \boldsymbol{e}_2 \\ \omega\dot{\boldsymbol{e}}_2 = \dot{\boldsymbol{x}}_2 - \dot{\hat{\boldsymbol{x}}}_2 = -\dfrac{a_2}{\omega^2}(\boldsymbol{x}_1 - \hat{\boldsymbol{x}}_1) + \boldsymbol{\chi} - \hat{\boldsymbol{\chi}} = -a_2\boldsymbol{e}_1 + \boldsymbol{e}_3 \\ \omega\dot{\boldsymbol{e}}_3 = \omega\left(\dot{\boldsymbol{\chi}} - \dot{\hat{\boldsymbol{\chi}}}\right) = -\dfrac{a_3}{\omega^2}(\boldsymbol{x}_1 - \hat{\boldsymbol{x}}_1) + \omega\dot{\boldsymbol{\chi}} = -a_3\boldsymbol{e}_1 + \omega\dot{\boldsymbol{\chi}} \end{cases} \tag{15}$$

then the observer error equations (15) can beexpressed by

$$\omega\dot{\boldsymbol{E}} = \boldsymbol{A}\boldsymbol{E} + \omega\boldsymbol{B}\dot{\boldsymbol{\chi}} \tag{16}$$

where

$$\boldsymbol{A} = \begin{bmatrix} -a_1\boldsymbol{I}_3 & \boldsymbol{I}_3 & 0_3 \\ -a_2\boldsymbol{I}_3 & 0_3 & \boldsymbol{I}_3 \\ -a_3\boldsymbol{I}_3 & 0_3 & 0_3 \end{bmatrix},\ \boldsymbol{B} = \begin{bmatrix} 0_3 \\ 0_3 \\ \boldsymbol{I}_3 \end{bmatrix}$$

To analyze the stability of(16), for any given positive definite matrix $\boldsymbol{Q}$,there exists a symmetric positive definite matrix $\boldsymbol{P}$satisfying the following Lyapunov equation.

$$\boldsymbol{A}^T\boldsymbol{P} + \boldsymbol{P}\boldsymbol{A} = -\boldsymbol{Q} \tag{17}$$

Theorem 1. Suppose that Assumption 4and the equation(17)are satisfied, then the observer error dynamics (16) isinput-to-state stable and the observation errorvector$\boldsymbol{E}$can converge to the origin.

Proof. The Lyapunov function candidateof the observer is defined as follows

$$V_o = \omega \boldsymbol{E}^T \boldsymbol{P} \boldsymbol{E} \tag{18}$$

The time derivative of V_o can be written as:

$$\begin{aligned}
\dot{V}_o &= \omega \dot{\boldsymbol{E}}^T \boldsymbol{P} \boldsymbol{E} + \omega \boldsymbol{E}^T \boldsymbol{P} \dot{\boldsymbol{E}} \\
&= \left(\boldsymbol{A}\boldsymbol{E} + \omega \boldsymbol{B} \dot{\boldsymbol{\chi}} \right)^T \boldsymbol{P} \boldsymbol{E} + \boldsymbol{E}^T \boldsymbol{P} \left(\boldsymbol{A}\boldsymbol{E} + \omega \boldsymbol{B} \dot{\boldsymbol{\chi}} \right) \\
&= \boldsymbol{E}^T \boldsymbol{A}^T \boldsymbol{P} \boldsymbol{E} + \omega \left(\boldsymbol{B} \dot{\boldsymbol{\chi}} \right)^T \boldsymbol{P} \boldsymbol{E} + \boldsymbol{E}^T \boldsymbol{P} \boldsymbol{A} \boldsymbol{E} + \omega \boldsymbol{E}^T \boldsymbol{P} \boldsymbol{B} \dot{\boldsymbol{\chi}} \\
&= \boldsymbol{E}^T \left(\boldsymbol{A}^T \boldsymbol{P} + \boldsymbol{P} \boldsymbol{A} \right) \boldsymbol{E} + 2\omega \boldsymbol{E}^T \boldsymbol{P} \boldsymbol{B} \dot{\boldsymbol{\chi}} \\
&\le -\boldsymbol{E}^T \boldsymbol{Q} \boldsymbol{E} + 2\omega \left\| \boldsymbol{P} \boldsymbol{B} \right\| \cdot \left\| \boldsymbol{E} \right\| \cdot \left\| \dot{\boldsymbol{\chi}} \right\| \\
&\le -\lambda_{\min} \left(\boldsymbol{Q} \right) \left\| \boldsymbol{E} \right\|^2 + 2\omega H \left\| \boldsymbol{P} \boldsymbol{B} \right\| \cdot \left\| \boldsymbol{E} \right\| \\
&\le -\varpi \left\| \boldsymbol{E} \right\|^2
\end{aligned} \tag{19}$$

where

$$\varpi = \lambda_{\min} \left(\boldsymbol{Q} \right) - \frac{2\omega H \left\| \boldsymbol{P} \boldsymbol{B} \right\|}{\left\| \boldsymbol{E} \right\|} \tag{20}$$

and $\lambda_{\min} \left(\boldsymbol{Q} \right)$ is the minimum eigenvalue of $\boldsymbol{Q}$.

To ensure $\varpi \ge 0$, and $\dot{V}_o \le 0$,the convergence condition of the observer can be obtained as:

$$\left\| \boldsymbol{E} \right\| \ge \frac{2\omega H \left\| \boldsymbol{P} \boldsymbol{B} \right\|}{\lambda_{\min} \left(\boldsymbol{Q} \right)} \tag{21}$$

By solving inequality(19),we obtain

$$0 \le V_o \le V(0) e^{-\varpi t} \tag{22}$$

Therefore, it can be seen that V_o is ultimately bounded, and the observer error dynamics(16) is input-to-state stable.

Remark 2. It can be seen from (21), the convergence rate of observation error $\left\| \boldsymbol{E} \right\|$is related to the parameter ω .The smaller ω , the faster $\left\| \boldsymbol{E} \right\|$ will converge.As ω decreases, the observation error $\left\| \boldsymbol{E} \right\|$will gradually approach zero.

Based on the above analysis and refer to (Wang et al., 2018), the following nonlinear ESO is designed in this paper.

$$\begin{cases} \tilde{\boldsymbol{\eta}} = \boldsymbol{x}_1 - \hat{\boldsymbol{x}}_1 \\ \dot{\hat{\boldsymbol{x}}}_1 = \hat{\boldsymbol{x}}_2 + \boldsymbol{\Lambda}_1 \tilde{\boldsymbol{\eta}} \\ \dot{\hat{\boldsymbol{x}}}_2 = \hat{\boldsymbol{\chi}} + \boldsymbol{\Lambda}_2 \boldsymbol{fal}\left(\tilde{\boldsymbol{\eta}}, \alpha_1, \delta_1\right) + \boldsymbol{R}(\psi)\boldsymbol{M}^{-1}\boldsymbol{\tau} \\ \dot{\hat{\boldsymbol{\chi}}} = \boldsymbol{\Lambda}_3 \boldsymbol{fal}\left(\tilde{\boldsymbol{\eta}}, \alpha_2, \delta_2\right) \end{cases} \tag{23}$$

where $\boldsymbol{\Lambda}_i \in \Re^{3\times 3}, i = 1,2,3$ is the positive real diagonal matrix, which is the gain matrix of observererror. $\boldsymbol{fal}\left(\tilde{\boldsymbol{\eta}}, \alpha, \delta\right)$ is the nonlinear function of the stateestimate error $\tilde{\boldsymbol{\eta}}$, which is defined as follows

$$fal\left(\tilde{\eta}_i, \alpha, \delta\right) = \begin{cases} \tilde{\eta}_i / \delta^{1-\alpha} & \left|\tilde{\eta}_i\right| \le \delta \\ sig^{\alpha}(\tilde{\eta}_i) & \left|\tilde{\eta}_i\right| \ge \delta \end{cases}, \ i = 1,2,3 \tag{24}$$

where $sig^{\alpha}(\tilde{\eta}_i) = sign(\tilde{\eta}_i)\left|\tilde{\eta}_i\right|^{\alpha}$, $0 \le \alpha, \delta < 1$.

Remark 3. The characteristics of $fal\left(\tilde{\eta}, \alpha, \delta\right)$ determine that the ESO is continuous and non-smooth, and has strong adaptability to model uncertainties and external disturbances.At the same time, its characteristics are directly affected by α and δ, where δ affects the slope of $fal\left(\tilde{\eta}, \alpha, \delta\right)$ and α affects the magnitude of $fal\left(\tilde{\eta}, \alpha, \delta\right)$.In this paper, we analyze the relationship between α and $fal\left(\tilde{\eta}, \alpha, \delta\right)$ when δ=0.01 by simulation.The simulation resultsare shown in Fig. 3.

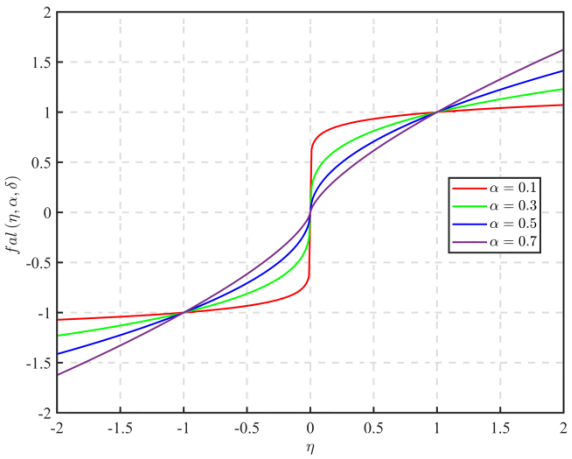

Fig. 3. The relationship between α and $fal\left(\tilde{\eta}, \alpha, \delta\right)$.

It can be seen from the analysis of Fig 3thatwhen $\left|\tilde{\eta}\right| \le \delta < 1$ and $\delta < \left|\tilde{\eta}\right| < 1$, then the larger α, the smaller $fal\left(\tilde{\eta}, \alpha, \delta\right)$ will be; when $\left|\tilde{\eta}\right| > 1$, if α is smaller, then $fal\left(\tilde{\eta}, \alpha, \delta\right)$ will be smaller.Therefore, by selecting appropriate design parameters, the fast convergence of the ESO can be achieved.

According to the nonlinear ESO(23) and the USV mathematical model(5), wecan obtain

$$\hat{\boldsymbol{\eta}} = \hat{\boldsymbol{x}}_1, \quad \hat{\boldsymbol{\upsilon}} = \boldsymbol{R}^{-1}(\psi)\hat{\boldsymbol{x}}_2 \tag{25}$$

where $\hat{\boldsymbol{\eta}} = \left[\hat{x}, \hat{y}, \hat{\psi}\right]^T$ represents the position observation vector of the USV, and

$\hat{\boldsymbol{\upsilon}} = [\hat{u}, \hat{v}, \hat{r}]^T$ denotes the velocity observation vector of the USV.In addition, $\tilde{\boldsymbol{\upsilon}} = \hat{\boldsymbol{\upsilon}} - \boldsymbol{\upsilon}$ denotes the velocity observation vector error.

3.2Design of the virtual control law

In general, the purpose of the trajectory tracking control is to follow the reference trajectory by adjusting the controller according to the position error.To facilitate the design of the trajectory tracking control law, the position tracking error is defined as:

$$x_e = x - x_d, \quad y_e = y - y_d \tag{26}$$

where (x_d, y_d) is the desired trajectorycoordinate of theUSV.

Differentiating (26) with respect to time yields

$$\begin{aligned} \dot{x}_e &= \hat{u}\cos\psi - \hat{v}\sin\psi - \dot{x}_d \\ \dot{y}_e &= \hat{u}\sin\psi + \hat{v}\cos\psi - \dot{y}_d \end{aligned} \tag{27}$$

Considering the Lyapunov function V_0 as follows

$$V_0 = \frac{1}{2}(x_e^2 + y_e^2) \tag{28}$$

Taking the time derivative of(28) along(27) yields

$$\begin{aligned} \dot{V}_0 &= x_e\dot{x}_e + y_e\dot{y}_e \\ &= x_e(\hat{u}\cos\psi - \hat{v}\sin\psi - \dot{x}_d) + y_e(\hat{u}\sin\psi + \hat{v}\cos\psi - \dot{y}_d) \end{aligned} \tag{29}$$

where $\hat{u}$ and $\hat{v}$ are regarded as the virtual control quantity. In order to make $\dot{V}_0$ negative and achieve the tracking error approaching zero,the virtual control law u_d and v_d aredefined as follows

$$\begin{bmatrix} u_d \\ v_d \end{bmatrix} = J(\psi)^{-1}\begin{bmatrix} \dot{x}_d - kx_e/\nabla \\ \dot{y}_d - ky_e/\nabla \end{bmatrix} \tag{30}$$

with

$$J(\psi) = \begin{bmatrix} \cos\psi & -\sin\psi \\ \sin\psi & \cos\psi \end{bmatrix} \text{ and } \nabla = \sqrt{x_e^2 + y_e^2 + C}\,.$$

where *k* and *C* are positivedesigned constants.

Remark 4. In (30), ∇ is introduced to prevent $|x_e|$ and $|y_e|$ from being too large,which may cause u_d and v_d exceed the reasonable speed range of the USV, resulting in system instability and even controller crash(Qiu et al., 2019).

Substituting (30) into(27), we obtain

$$\begin{bmatrix} \dot{x}_e \\ \dot{y}_e \end{bmatrix} = J(\psi)\begin{bmatrix} \hat{u} - u_d \\ \hat{v} - v_d \end{bmatrix} + \begin{bmatrix} -kx_e/\nabla \\ -kx_e/\nabla \end{bmatrix} \tag{31}$$

It can be seen from (31) thatwhen $\hat{u} \to u_d$ and $\hat{v} \to v_d$, the position error will also converge to zero gradually.

The time derivative of (30) can be described as:

$$\begin{cases} \dot{u}_d = rv_d + H_1 \cos\psi + H_2 \sin\psi \\ \dot{v}_d = -ru_d - H_1 \sin\psi + H_2 \cos\psi \end{cases} \tag{32}$$

with

$$\begin{cases} H_1 = \ddot{x}_d - k\dot{x}_e(\nabla^{-1} - \nabla^{-3}x_e^2) + k\nabla^{-3}x_e y_e \dot{y}_e \\ H_2 = \ddot{y}_d - k\dot{y}_e(\nabla^{-1} - \nabla^{-3}y_e^2) + k\nabla^{-3}x_e y_e \dot{x}_e \end{cases}.$$

It can be seen from (32) that $\dot{u}_d$ and $\dot{v}_d$ are quite complex. Therefore, to avoid the "differential explosion" caused by the direct derivation of the virtual control law in the next step, we let u_d and v_d pass through the following neural shunt model to obtain the new controlvariables β_u and β_v.

$$\begin{aligned} \dot{\beta}_u &= -A_u\beta_u + (B_u - \beta_u)f(u_d) - (D_u + \beta_u)g(u_d) \\ \dot{\beta}_v &= -A_v\beta_v + (B_v - \beta_v)f(v_d) - (D_v + \beta_v)g(v_d) \end{aligned} \tag{33}$$

where A_i, B_i and D_i, $i = u, v$, have the same meaning as defined by(Pan et al., 2015). $f(x)$ and $g(x)$ are linear threshold functions, which can be defined as:

$$f(x) = \max\{x, 0\}, \quad g(x) = \max\{-x, 0\} \tag{34}$$

Define the new error variables y_u and y_v as:

$$\begin{aligned} y_u &= \beta_u - u_d \\ y_v &= \beta_v - v_d \end{aligned} \tag{35}$$

whose time derivative along (33) can be expressed by

$$\begin{aligned} \dot{y}_u &= \dot{\beta}_u - \dot{u}_d \\ &= -\left[A_u + f(u_d) + g(u_d)\right]\beta_u + \left[B_u f(u_d) - D_u g(u_d)\right] - Y_u \\ \dot{y}_v &= \dot{\beta}_v - \dot{v}_d \\ &= -\left[A_v + f(v_d) + g(v_d)\right]\beta_v + \left[B_v f(v_d) - D_v g(v_d)\right] - Y_v \end{aligned} \tag{36}$$

with

$$Y_u = \frac{\partial u_d}{\partial x}\dot{x} + \frac{\partial u_d}{\partial x_d}\dot{x}_d + \frac{\partial u_d}{\partial \dot{x}_d}\ddot{x}_d + \frac{\partial u_d}{\partial y}\dot{y} + \frac{\partial u_d}{\partial y_d}\dot{y}_d + \frac{\partial u_d}{\partial \psi}\dot{\psi}$$

$$Y_v = \frac{\partial v_d}{\partial x}\dot{x} + \frac{\partial v_d}{\partial x_d}\dot{x}_d + \frac{\partial v_d}{\partial \dot{y}_d}\ddot{y}_d + \frac{\partial v_d}{\partial y}\dot{y} + \frac{\partial v_d}{\partial y_d}\dot{y}_d + \frac{\partial v_d}{\partial \psi}\dot{\psi}.$$

From the definition of functions $f(u_d)$ and $g(u_d)$, we have $f(u_d) > 0$ and $f(v_d) > 0$. If $u_d \geq 0$, then $f(u_d) = u_d$ and $g(u_d) = 0$; if $u_d < 0$, then $f(u_d) = 0$ and $g(u_d) = -u_d$. Hence, by choosing $B_i = D_i, i = u, v$, then (36)can be simplified as:

$$\dot{y}_u = \dot{\beta}_u - \dot{u}_d = -M_u\beta_u + B_u u_d - Y_u \tag{37}$$
$$\dot{y}_v = \dot{\beta}_v - \dot{v}_d = -M_v\beta_v + B_v v_d - Y_v$$

where $M_u = A_u + f(u_d) + g(u_d) > 0$ and $M_v = A_v + f(v_d) + g(v_d) > 0$.

Assumption 5 (Mu et al., 2017)**.**Assume Y_u and Y_v are bounded and satisfy $Y_u \le \overline{Y}_u$ and $Y_v \le \overline{Y}_v$, where $\overline{Y}_u$ and $\overline{Y}_v$ are positive constants.

3.3Design of adaptive NTSM controller

In this subsection,an adaptive NTSM controllerfor the underactuated USVbased on MLP and ESO is introduced to design surgemotion control law τ_u and yaw motion control law τ_r. To put it simply,we design τ_u and τ_r to forcethe actual surge and yaw velocities to track the virtual control law(30), and itsstability is analyzed by Lyapunov stability theory.

Step 1: Define the surgevelocity error $u_e = \hat{u} - u_d$, andintroduce the NTSM surface for the surge velocity error u_e as:

$$s_1 = u_e + \lambda_1 \int_0^t u_e(t)dt + \beta_1 sig^{\frac{p_1}{q_1}}(u_e) \tag{38}$$

where $\lambda_1 > 0$, $\beta_1 > 0$, $1 < p_1/q_1 < 2$, p_1 and q_1 are both positive integers.

Taking thetime derivative of (38) produces

$$\begin{aligned}\dot{s}_1 &= \dot{u}_e + \lambda_1 u_e + \frac{\beta_1 p_1}{q_1}\dot{u}_e |u_e|^{\frac{p_1}{q_1}-1} \\ &= \left[\frac{\beta_1 p_1}{q_1}|u_e|^{\frac{p_1}{q_1}-1} + 1\right]\dot{u}_e + \lambda_1 u_e \\ &= \frac{\beta_1 p_1 |u_e|^{\frac{p_1}{q_1}-1} + q_1}{q_1}\left[\frac{1}{m_{11}}\left(m_{22}\hat{v}\hat{r} - d_{11}\hat{u} + \Delta f_u + \tau_{\mathrm{cu}} + \tau_{\mathrm{du}} - m_{11}\dot{\beta}_u\right)\right] + \lambda_1 u_e\end{aligned} \tag{39}$$

In Equation(39), Δf_u is the uncertainty term of the USV model. In this paper,we choose the MLP method instead of the RBF neural networkto approximate the unknown function Δf_u to simplify calculations(Shen et al., 2020a).Define $\phi = \|W^*\|^2$, where $\hat{\phi}$ is the estimation of ϕ and $\tilde{\phi} = \phi - \hat{\phi}$ representsestimation error. In addition, to reduce the chattering problem and the influence of disturbances,the sliding modecontrol law is designed by using the hyperbolic tangent function, which can be expressed as:

$$\dot{s}_1 = -\hat{\tau}_{du}^{\max}\tanh(s_1/\varepsilon_1) - \eta_1 s_1 \tag{40}$$

where ε_1 and η_1 are positive design parameters, $\hat{\tau}_{du}^{\max}$ is the estimated upper bound value of uncertain external ocean disturbances, and the corresponding estimated error is $\tilde{\tau}_{du}^{\max} = \hat{\tau}_{du}^{\max} - \tau_{du}^{\max}$.

Then the surge motion NTSM control law can be designed as:

$$\tau_{cu} = -m_{22}\hat{v}\hat{r} + d_{11}\hat{u} - \Delta\hat{f}_u + m_{11}\dot{\beta}_u - \frac{m_{11}\lambda_1 u_e q_1}{\beta_1 p_1 |u_e|^{\frac{p_1}{q_1}-1} + q_1} - \frac{q_1}{\beta_1 p_1 |u_e|^{\frac{p_1}{q_1}-1} + q_1}\left[\hat{\tau}_{du}^{\max}\tanh(s_1/\varepsilon_1) + \eta_1 s_1\right] \tag{41}$$

where $\Delta\hat{f}_u = \frac{1}{2}s_1\hat{\phi}_1 hh^T$ is the estimate of Δf_u.

The update law for $\hat{\phi}_1$ and the adaptive law for $\hat{\tau}_{du}^{\max}$ can be designedas:

$$\dot{\hat{\phi}}_1 = \Gamma_1\left[\frac{1}{2}s_1^2 hh^T - \vartheta_1\hat{\phi}_1\right] \tag{42}$$

$$\dot{\hat{\tau}}_{du}^{\max} = \gamma_1\left[s_1\tanh(s_1/\varepsilon_1) - \mu_1(\hat{\tau}_{du}^{\max} - \tau_{du}^0)\right] \tag{43}$$

where Γ_1, γ_1, ϑ_1 and μ_1 are positive design parameters, τ_{du}^0 is the initial value of the related variable.

Taking into account the input saturationproblem, the final surge control law can be described as:

$$\tau_u = \begin{cases} sign(\tau_{cu})\tau_{u\max}, & |\tau_{cu}| > \tau_{u\max} \\ \tau_{cu}, & |\tau_{cu}| \le \tau_{u\max} \end{cases} \tag{44}$$

Remark 5. It should be pointed out thatthe hyperbolic tangent function is introduced to replacethe sign function to design the sliding mode control law, which can not onlyeffectively eliminate the adverse effect caused by chattering, but also ensures that the tracking errors converge to zero.

Step 2: Define theyaw velocity error $v_e = \hat{v} - v_d$, andintroduce the NTSM surface for the yaw velocity error v_e as:

$$s_2 = v_e + \beta_2 sig^{\frac{p_2}{q_2}}(\dot{v}_e) \tag{45}$$

where $\beta_2 > 0$, $1 < p_2/q_2 < 2$, p_2 and q_2 are both positive integers.

Taking the time derivative of (45)yields

$$\dot{s}_2 = \dot{v}_e + \frac{\beta_2 p_2}{q_2}\ddot{v}_e|\dot{v}_e|^{\frac{p_2}{q_2}-1} = \frac{\beta_2 p_2}{q_2}|\dot{v}_e|^{\frac{p_2}{q_2}-1}\left\{\frac{u_d}{m_{33}}\left[(m_{11}-m_{22})\hat{u}\hat{v} - d_{33}\hat{r} + \Delta f_r + \tau_{cr} + \tau_{dr} + \frac{m_{33}}{u_d}(\ddot{\hat{v}} + \hat{r}\dot{\beta}_v - \dot{F}_2)\right]\right\} + \dot{v}_e \tag{46}$$

where $F_2 = -H_1\sin\psi + H_2\cos\psi$.

Such as the surge motion controller design,we introduce MLP instead of RBF neural network to approximate the unknown function Δf_r. Meanwhile,the yaw motion sliding mode control law is designed by using the hyperbolic tangent function. Then the yaw motion NTSM control law can be designed as:

$$\begin{aligned}\tau_{cr} &= -(m_{11}-m_{22})\hat{u}\hat{v} + d_{33}\hat{r} - \Delta\hat{f}_r - \frac{m_{33}}{u_d}(\dot{\hat{v}} + \hat{r}\dot{\beta}_v - \dot{F}_2) \\ &- \frac{m_{33}q_2}{u_d\beta_2 p_2}\left|\dot{v}_e\right|^{2-\frac{p_2}{q_2}} - \frac{q_2}{\beta_2 p_2}\left|\dot{v}_e\right|^{1-\frac{p_2}{q_2}}\left[\hat{\tau}_{dr}^{\max}\tanh(s_2/\varepsilon_2) + \eta_2 s_2\right]\end{aligned} \tag{47}$$

where $\Delta\hat{f}_r = 1/2\times s_2\hat{\phi}_2 hh^T$ is the estimate of Δf_r. $\hat{\tau}_{dr}^{\max}$ is the estimated upper bound value of uncertain external ocean disturbances, and the corresponding estimated error is $\tilde{\tau}_{dr}^{\max} = \hat{\tau}_{dr}^{\max} - \tau_{dr}^{\max}$. ε_2 and η_2 are positive design parameters.

The update law for $\hat{\phi}_2$ and the adaptive law for $\hat{\tau}_{dr}^{\max}$ can be designedas:

$$\dot{\hat{\phi}}_2 = \Gamma_2\left[\frac{1}{2}s_2^2 hh^T - \vartheta_2\hat{\phi}_2\right] \tag{48}$$

$$\dot{\hat{\tau}}_{dr}^{\max} = \gamma_2\left[s_2\tanh(s_2/\varepsilon_2) - \mu_2(\hat{\tau}_{dr}^{\max} - \tau_{dr}^{0})\right] \tag{49}$$

where Γ_2, γ_2, ϑ_2 and μ_2 are positive design parameters, τ_{dr}^{0} is the initial value.

Taking into account the input saturationproblem, the final yaw motion control law can be described as:

$$\tau_r = \begin{cases} sign(\tau_{cr})\tau_{r\max}, & \left|\tau_{cr}\right| > \tau_{r\max} \\ \tau_{cr}, & \left|\tau_{cr}\right| \le \tau_{r\max} \end{cases} \tag{50}$$

Remark 6. It is worth mentioning thatby introducing the MLP method, we can see that we only need to estimate the two constants ϕ_1 and ϕ_2. Therefore, the calculation burden is effectively reduced and the real-time and robust performance of the control system is greatly improved.Moreover,by incorporating the neural shuntdynamicsmodel, which avoids directly deriving the virtual control signals (u_d and v_d) and improves the computational efficiency of the tracking control algorithm, and also realizes the application from the biological field to other fields.

Based on the above controller design, the main result of this paper is summarized as Theorem 2.

Theorem 2. Consider the closed-loop system consisting of the underactuated USV dynamics(5) or (10)obeying Assumptions 1–5,the NTSM controllaws(44),(50), the MLP neuralnetwork update laws(42),(48), the adaptive laws(43),(49), the neural shunt models (33), and simultaneously suffering fromthe model parametric uncertainties, unmeasurable velocitiesand unknown external ocean disturbances.By choosingappropriate design parameters, such that all tracking error signals inthe closed-loop system fast converge to a small neighborhood of the origin that can be made arbitrarily small.

Proof. Consider the candidate Lyapunov function *V* as follows:

$$V = \frac{1}{2}m_{11}s_1^2 + \frac{1}{2}m_{33}s_2^2 + \frac{1}{2\gamma_1}\tilde{\tau}_{du}^{\max 2} + \frac{1}{2\gamma_2}\tilde{\tau}_{dr}^{\max 2} + \frac{1}{2\Gamma_1}\tilde{\phi}_1^2 + \frac{1}{2\Gamma_2}\tilde{\phi}_2^2 + \frac{1}{2}y_u^2 + \frac{1}{2}y_v^2 \tag{51}$$

Then, taking the time derivative $\dot{V}$ along(39)，(46)，(43)，(49)，(42)，(48)，(37)，andsubmitting the control laws(41) and(47), we have

$$\begin{aligned}\dot{V} &= m_{11}s_1\dot{s}_1 + m_{33}s_2\dot{s}_2 + \gamma_1^{-1}\tilde{\tau}_{du}^{\max}\dot{\hat{\tau}}_{du}^{\max} + \gamma_2^{-1}\tilde{\tau}_{dr}^{\max}\dot{\hat{\tau}}_{dr}^{\max} - \Gamma_1^{-1}\tilde{\phi}_1\dot{\hat{\phi}}_1 - \Gamma_2^{-1}\tilde{\phi}_2\dot{\hat{\phi}}_2 + y_u\dot{y}_u + y_v\dot{y}_v \\ &= s_1\left[W_u^{*T}h + \varsigma_u - \frac{1}{2}s_1\hat{\phi}_1 hh^T + \tau_{du} - \hat{\tau}_{du}^{\max}\tanh(s_1/\varepsilon_1) - \eta_1 s_1\right] \\ &\quad + s_2\left[W_r^{*T}h + \varsigma_r - \frac{1}{2}s_2\hat{\phi}_2 hh^T + \tau_{dr} - \hat{\tau}_{dr}^{\max}\tanh(s_2/\varepsilon_2) - \eta_2 s_2\right] \\ &\quad + \tilde{\tau}_{du}^{\max}\left[s_1\tanh(s_1/\varepsilon_1) - \mu_1(\hat{\tau}_{du}^{\max} - \tau_{du}^0)\right] + \tilde{\tau}_{dr}^{\max}\left[s_2\tanh(s_2/\varepsilon_2) - \mu_2(\hat{\tau}_{dr}^{\max} - \tau_{dr}^0)\right] \\ &\quad - \Gamma_1^{-1}\tilde{\phi}_1\dot{\hat{\phi}}_1 - \Gamma_2^{-1}\tilde{\phi}_2\dot{\hat{\phi}}_2 + y_u\dot{y}_u + y_v\dot{y}_v \\ &\le s_1W_u^{*T}h + s_2W_r^{*T}h + s_1\varsigma_u + s_2\varsigma_r - \frac{1}{2}s_1^2\hat{\phi}_1 hh^T - \frac{1}{2}s_2^2\hat{\phi}_2 hh^T - \Gamma_1^{-1}\tilde{\phi}_1\dot{\hat{\phi}}_1 - \Gamma_2^{-1}\tilde{\phi}_2\dot{\hat{\phi}}_2 \\ &\quad + \tau_{du}^{\max}\left[|s_1| - s_1\tanh(s_1/\varepsilon_1)\right] + \tau_{dr}^{\max}\left[|s_2| - s_2\tanh(s_2/\varepsilon_2)\right] - \eta_1 s_1^2 - \eta_2 s_2^2 \\ &\quad - \mu_1\tilde{\tau}_{du}^{\max}(\hat{\tau}_{du}^{\max} - \tau_{du}^0) - \mu_2\tilde{\tau}_{dr}^{\max}(\hat{\tau}_{dr}^{\max} - \tau_{dr}^0) + y_u\dot{y}_u + y_v\dot{y}_v\end{aligned} \tag{52}$$

According to Lemma 1,we can get $|s_i| - s_i\tanh(s_i/\varepsilon_i) \le \kappa\varepsilon_i$, $i = 1,2$, and from Young's inequality, we havethe following inequalities:

$$\begin{aligned}-\mu_1\tilde{\tau}_{du}^{\max}(\hat{\tau}_{du}^{\max} - \tau_{du}^0) &\le -\frac{\mu_1}{2}\tilde{\tau}_{du}^{\max 2} + \frac{\mu_1}{2}(\tau_{du}^{\max} - \tau_{du}^0)^2 \\ -\mu_2\tilde{\tau}_{dr}^{\max}(\hat{\tau}_{dr}^{\max} - \tau_{dr}^0) &\le -\frac{\mu_2}{2}\tilde{\tau}_{dr}^{\max 2} + \frac{\mu_2}{2}(\tau_{dr}^{\max} - \tau_{dr}^0)^2\end{aligned} \tag{53}$$

$$\begin{aligned}s_1W_u^{*T}h &\le \frac{1}{2}s_1^2\phi_1 hh^T + \frac{1}{2} \\ s_2W_r^{*T}h &\le \frac{1}{2}s_2^2\phi_2 hh^T + \frac{1}{2}\end{aligned} \tag{54}$$

$$\begin{aligned}s_1\varsigma_u &\le \frac{s_1^2}{2} + \frac{\varsigma_u^2}{2} \le \frac{s_1^2}{2} + \frac{\varsigma_U^2}{2} \\ s_2\varsigma_r &\le \frac{s_2^2}{2} + \frac{\varsigma_r^2}{2} \le \frac{s_2^2}{2} + \frac{\varsigma_R^2}{2}\end{aligned} \tag{55}$$

Then, substituting(53), (54), (55)and (37)into (52)yields

$$\begin{aligned}\dot{V} &\le -\frac{2\eta_1 - 1}{2}s_1^2 - \frac{2\eta_2 - 1}{2}s_2^2 + \tilde{\phi}_1\left(\frac{1}{2}s_1^2 hh^T - \Gamma_1^{-1}\dot{\hat{\phi}}_1\right) + \tilde{\phi}_2\left(\frac{1}{2}s_2^2 hh^T - \Gamma_2^{-1}\dot{\hat{\phi}}_2\right) \\ &\quad + \kappa\varepsilon_1\tau_{du}^{\max} + \kappa\varepsilon_2\tau_{dr}^{\max} + \frac{\varsigma_U^2}{2} + \frac{\varsigma_R^2}{2} - \frac{\mu_1}{2}\tilde{\tau}_{du}^{\max 2} - \frac{\mu_2}{2}\tilde{\tau}_{dr}^{\max 2} + \frac{\mu_1}{2}(\tau_{du}^{\max} - \tau_{du}^0)^2 \\ &\quad + \frac{\mu_2}{2}(\tau_{dr}^{\max} - \tau_{dr}^0)^2 + 1 - y_u(M_u\beta_u - B_u u_d) - y_v(M_v\beta_v - B_v v_d) - y_u Y_u - y_v Y_v\end{aligned} \tag{56}$$

We define $M_u = B_u$, $M_v = B_v$, then get $M_u\beta_u - B_u u_d = M_u y_u$, $M_v\beta_v - B_v v_d = M_v y_v$.

Thus, (56) can be written as:

$$\begin{aligned}\dot{V} \le & -\frac{2\eta_1-1}{2}s_1^2-\frac{2\eta_2-1}{2}s_2^2+\vartheta_1\tilde{\phi}_1\hat{\phi}_1+\vartheta_2\tilde{\phi}_2\hat{\phi}_2+\kappa\varepsilon_1\tau_{du}^{\max}+\kappa\varepsilon_2\tau_{dr}^{\max} \\ & -\frac{\mu_1}{2}\tilde{\tau}_{du}^{\max 2}-\frac{\mu_2}{2}\tilde{\tau}_{dr}^{\max 2}+\frac{\varsigma_U^2}{2}+\frac{\varsigma_R^2}{2}+\frac{\mu_1}{2}(\tau_{du}^{\max}-\tau_{du}^{0})^2+\frac{\mu_2}{2}(\tau_{dr}^{\max}-\tau_{dr}^{0})^2+1 \\ & -M_u y_u^2-M_v y_v^2-y_u Y_u-y_v Y_v\end{aligned} \tag{57}$$

Because $\left(\tilde{\phi}_i-\phi_i\right)^2=\tilde{\phi}_i^2+\phi_i^2-2\tilde{\phi}_i\left(\hat{\phi}_i+\tilde{\phi}_i\right)\ge 0$, then we can obtain $2\tilde{\phi}_i\hat{\phi}_i\le\phi_i^2-\tilde{\phi}_i^2$, where $i=1,2$. From Young's inequality, i.e., $ab\le\frac{1}{2\sigma}a^2+\frac{\sigma}{2}b^2$ with $\sigma>0$ and $(a,b)\in\Re^2$. It follows that

$$\begin{aligned}-y_u Y_u &\le \frac{\sigma_u y_u^2}{2}+\frac{\bar{Y}_u^2}{2\sigma_u} \\ -y_v Y_v &\le \frac{\sigma_v y_v^2}{2}+\frac{\bar{Y}_v^2}{2\sigma_v}\end{aligned} \tag{58}$$

where σ_u and σ_v are positive constants.

Then (57)can be written as:

$$\begin{aligned}\dot{V} \le & -\frac{2\eta_1-1}{2}s_1^2-\frac{2\eta_2-1}{2}s_2^2-\frac{\mu_1}{2}\tilde{\tau}_{du}^{\max 2}-\frac{\mu_2}{2}\tilde{\tau}_{dr}^{\max 2}-\frac{\vartheta_1}{2}\tilde{\phi}_1^2-\frac{\vartheta_2}{2}\tilde{\phi}_2^2 \\ & -\frac{2M_u-\sigma_u}{2}y_u^2-\frac{2M_v-\sigma_v}{2}y_v^2+\kappa\varepsilon_1\tau_{du}^{\max}+\kappa\varepsilon_2\tau_{dr}^{\max}+\frac{\varsigma_U^2}{2}+\frac{\varsigma_R^2}{2} \\ & +\frac{\vartheta_1}{2}\phi_1^2+\frac{\vartheta_2}{2}\phi_2^2+\frac{\bar{Y}_u^2}{2\sigma_u}+\frac{\bar{Y}_v^2}{2\sigma_v}+\frac{\mu_1}{2}(\tau_{du}^{\max}-\tau_{du}^{0})^2+\frac{\mu_2}{2}(\tau_{dr}^{\max}-\tau_{dr}^{0})^2+1 \\ & \le -lV+Q\end{aligned} \tag{59}$$

where

$$l=\min\left\{2\eta_1-1,2\eta_2-1,\mu_1,\mu_2,\vartheta_1,\vartheta_2,2M_u-\sigma_u,2M_v-\sigma_v\right\}$$

$$\begin{aligned}Q=&\kappa\varepsilon_1\tau_{du}^{\max}+\kappa\varepsilon_2\tau_{dr}^{\max}+\frac{\varsigma_U^2}{2}+\frac{\varsigma_R^2}{2}+\frac{\vartheta_1}{2}\phi_1^2+\frac{\vartheta_2}{2}\phi_2^2+\frac{\bar{Y}_u^2}{2\sigma_u}+\frac{\bar{Y}_v^2}{2\sigma_v} \\ &+\frac{\mu_1}{2}(\tau_{du}^{\max}-\tau_{du}^{0})^2+\frac{\mu_2}{2}(\tau_{dr}^{\max}-\tau_{dr}^{0})^2+1\end{aligned}$$

$2\eta_1-1>0,\ 2\eta_2-1>0,\ 2M_u-\sigma_u>0,\ 2M_v-\sigma_v>0$.

Solving inequality(59) gives

$$0\le V(t)\le\frac{Q}{l}+\left[V(0)-\frac{Q}{l}\right]e^{-lt} \tag{60}$$

Since $\lim_{t\to\infty} V(t) = Q/l$, according to Lemma 2, we know $V(t)$ is uniformly ultimatelybounded.Inequality(60)confirms allthe error signals s_1, s_2, $\tilde{\tau}_{du}^{\max}$, $\tilde{\tau}_{dr}^{\max}$, $\tilde{\phi}_1$, $\tilde{\phi}_2$, y_u, y_v are uniformly ultimately bounded.Further, it can be seen that u_e and v_e are bounded, andthen from (31) we can see that x_e and y_e are also bounded.By selecting appropriate parameters, the quantity Q/l can be made arbitrarily small. Therefore, the tracking errors may be made arbitrarily small, thenthe USV can track trajectory accurately.

4. Numerical Simulations

In this section,numerical simulations are performed to validatethe effectiveness and superiority of the proposedNTSMC trajectory tracking scheme. The comparative simulation of the adaptive sliding mode control by employing MLP scheme (ASMC-MLP)proposed by(Qiu et al., 2019)is conducted on the underactuated USV. As shown inFig.4, the USV is a small intelligent marine vehicle with an overall length of6.4 m and breadth of 2.4 m.The vessel mainly consists of navigation, guidance andcontrol system, propulsion system, communication system, and sensing system including camera, RAR(radar angle reflector), and so on,which the propulsion system of the USV adopts an outboard propeller with the propulsionangle $\theta \in [-30^\circ, +30^\circ]$.The main parameters are listed in Table 1.

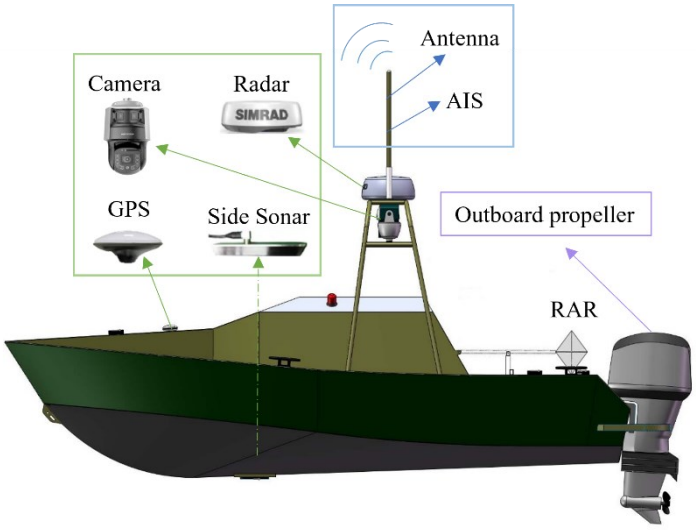

Fig. 4. The underactuated USV.

To testify the robustness and effectiveness of the proposed controller,the modeling uncertainties $\Delta \boldsymbol{f}$ and external time-varying disturbances $\boldsymbol{\tau}_d$ are assumed to be as follows:

$$\Delta \boldsymbol{f} = \begin{bmatrix} \Delta f_u \\ \Delta f_v \\ \Delta f_r \end{bmatrix} = 10^3 \times \begin{bmatrix} -0.2\times 0.83u^2 - 0.1\times 0.83u^3 \\ -0.2\times 2.55v^2 - 0.1\times 2.55v^3 \\ -0.2\times 1.25r^2 - 0.1\times 1.25r^3 \end{bmatrix} \tag{61}$$

$$\boldsymbol{\tau}_d = \begin{bmatrix} \tau_{du} \\ \tau_{dv} \\ \tau_{dr} \end{bmatrix} = \begin{bmatrix} 85\times\left[\sin(0.2t)+\cos(0.5t+\pi/4)+\sin(0.2t+\pi/6)\right] \\ 50\times\left[\sin(0.1t)+\cos(0.4t+\pi/4)+\sin(0.2t+\pi/6)\right] \\ 65\times\left[\sin(0.4t)+\cos(0.3t+\pi/4)+\sin(0.2t+\pi/6)\right] \end{bmatrix} \tag{62}$$

Table 1

The principle parameters of the underactuated USV.

Parameter	Value	Unit
m	1900	[kg]
m_{11}	2500	[kg]
m_{22}	3200	[kg]
m_{33}	980	[kg]
d_{11}	830	[kg]
d_{22}	2550	[kg]
d_{33}	1250	[kg]

In addition, the mean integrated absolute error (MIAE) index(Zhu and Du, 2020) is introduced to quantitativelyevaluateand compare the tracking performanceof the proposedNTSMC scheme and ASMC-MLPproposed in(Qiu et al., 2019), which can bedescribed as:

$$MIAE = \frac{1}{t_f - t_0}\int_{t_0}^{t_f} \left| j_e \right| dt \tag{63}$$

where j_e ($j = x, y, u, v$) represents the tracking errors, t_0 and t_f represent the start and end simulation times,respectively.

To make the trajectory tracking performance persuasive,the desired trajectory consists of a straight line and two circles, which can be described as:

$$\begin{aligned} x_d &= \begin{cases} 150+100\sin(0.04t) & (\ 0 \le t \le T_1) \\ 150+4(t-T_1) & (T_1 < t \le T_2) \\ 150+48\pi+100\sin[0.04(t-T_2)] & (T_2 < t \le T_3) \end{cases} \\ y_d &= \begin{cases} 100\sin(0.04t) & (\ 0 \le t \le T_1) \\ 0 & (T_1 < t \le T_2) \\ -100+100\cos[0.04(t-T_2)] & (T_2 < t \le T_3) \end{cases} \end{aligned} \tag{64}$$

where $T_1 = 50\pi$ s, $T_2 = 62\pi$ s, and $T_3 = 400$ s.

For better comparison of different experimental results of the trajectory tracking on different control methods, the initial states are set to be the same. The initial conditions are chosen as: $\boldsymbol{\eta}(0) = [150m, 20m, 0rad]^T$ and $\boldsymbol{\nu}(0) = [0\,m/s, 0\,m/s, 0\,rad/s]^T$ .The parameters of ESO, control laws,adaptive laws, and neural network update laws are properly selected in Table 2.The parameters of the MLP neural network with 39hidden

node numbers are designed in this paper. The width b_i of the Gaussian function affects the network mappingrange,for the inputs, the closer the c_i are to each other, the moresensitive the Gaussian function is. Thus, through multiple trials, we properly choose the widths to be $b_1 = 4.5$ and $b_2 = 1.8$, the center vector $\boldsymbol{c}_1$ evenlydistributed in $[-8,8]$ and $[-0.3,0.3]$. In addition, the parameters of the neural shunt model are chosen as: $A_u = A_v = 3$, $M_u = B_u = 3 + f(u_d) + g(u_d)$ and $M_v = B_v = 3 + f(v_d) + g(v_d)$. The magnitudes of the actuated forces and moments are specified in the ranges given by $\tau_u \in [-3.3\times10^3, 1.3\times10^4]$ and $\tau_r \in [-4.4\times10^2, 4.5\times10^2]$.

Table 2

The designed parameters of the controller.

Description	Value
Parameters of ESO	$\alpha_1 = 0.3, \alpha_2 = 0.2, \delta_1 = \delta_2 = 0.01$ $\boldsymbol{\Lambda}_1 = diag(30,30,30), \boldsymbol{\Lambda}_2 = diag(30,30,30)$ $\boldsymbol{\Lambda}_3 = diag(50,50,50)$
Parameters of control laws	$k = 1.2, C = 5, \lambda_1 = \lambda_2 = 1, \beta_1 = \beta_2 = 1$ $p_1 = p_2 = 5, q_1 = q_2 = 3, \eta_1 = 40, \eta_2 = 50$ $\varepsilon_1 = \varepsilon_2 = 0.1$
Parameters of adaptive laws	$\gamma_1 = 35$, $\gamma_2 = 35$, $\tau_{du}^0 = \tau_{dr}^0 = 0.1$ $\mu_1 = 1.4\times10^3$, $\mu_2 = 3.0\times10^3$
Parameters of update laws	$\Gamma_1 = 5$, $\Gamma_2 = 1$, $\vartheta_1 = 1.2\times10^{-6}$, $\vartheta_2 = 5\times10^{-4}$

In the same conditions, we confirm the advantages of the proposedscheme by comparison against the ASMC-MLP method proposed by(Qiu et al., 2019), and the simulationresults are sketched in Figs.5–14.Itcan be observed that the proposed NTSMC scheme has better tracking performance and effectiveness than the ASMC-MLP strategy subject to input saturationconstraints, model uncertainties,and external time-varying disturbances.

Fig. 5 depicts the simulation results of trajectory tracking comparison between the proposed scheme and the ASMC-MLP strategy under model uncertainties and external disturbances. Itcan be observed that both controllers can track the desired trajectory accurately, and the proposed scheme has better performance in terms of convergence rate at the initial stage of control.Fig. 6depicts the results of position tracking.In the meantime, the corresponding tracking errors are shown inFig. 7,which demonstratesthat the USV could track the reference positionin around the 30s and achieve faster error stabilization as compared to the ASMC-MLP strategy.Figs. 8–9 compare the velocity tracking results between the proposed scheme and the ASMC-MLP strategy, from the parts enlarged view we cansee that the velocity errors under the proposed schemecouldquickly converge to a small neighborhood around the origin and keep stable at the balanced point.Furthermore,to better present theperformance superiority of ourproposed controller in detail,the value of the MIAE index of position error x_e, y_e and velocity error u_e, v_e are listed in Table 3.

Table 3
The MIAE indexes of position error x_e , y_e and velocity error u_e , v_e under both controllers.

MIAE	x_e	y_e	u_e	v_e
The proposed scheme	0.0347	0.5536	0.0102	0.0188
ASMC-MLP scheme	0.0482	0.7790	0.0170	0.0230

Comparing these indexes in Table 3, it can be seen that the MIAE index of x_e of the proposed scheme is 72% of the ASMC-MLP scheme, the MIAE index of y_e of the proposed scheme is 71.9% of the ASMC-MLP scheme, the MIAE index of u_e of the proposed scheme is 60% of the ASMC-MLP scheme, the MIAE index of v_e of the proposed scheme is 81.7 % of the ASMC-MLP scheme. Therefore, the proposed NTSMC scheme has a lower MIAE index than the ASMC-MLP scheme, which reflects that the proposed scheme has better transientresponse performance and robustness.

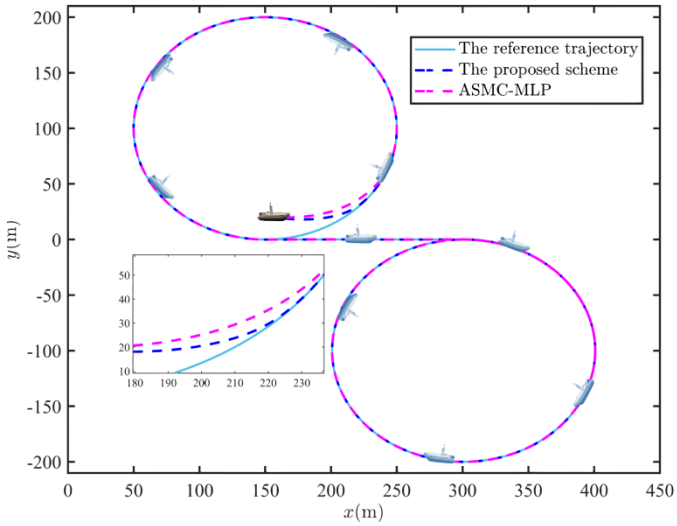

Fig. 5. The reference and actual trajectories in the x-y plane.

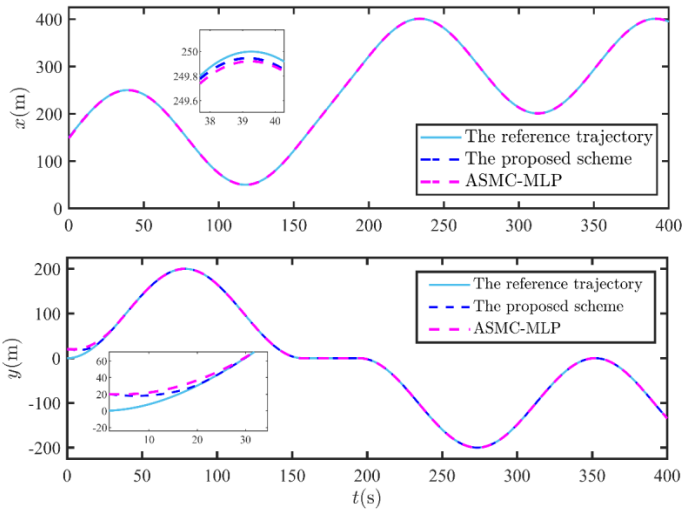

Fig. 6. The curves of reference and actual positions in the x-axis and the y-axis directions.

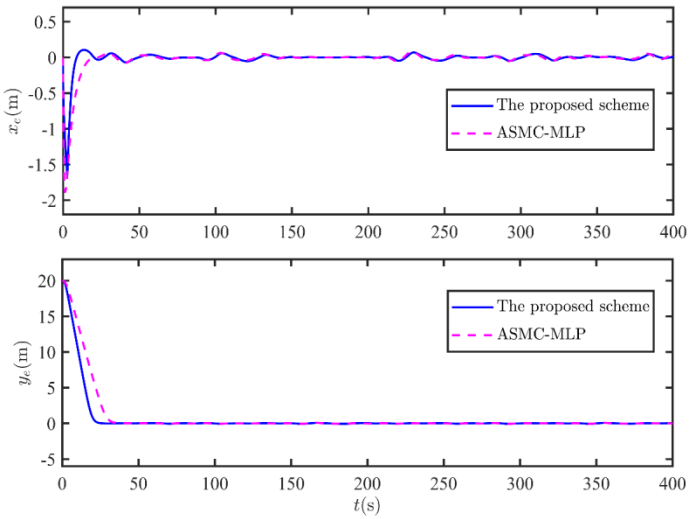

Fig. 7. The curves of position tracking errors.

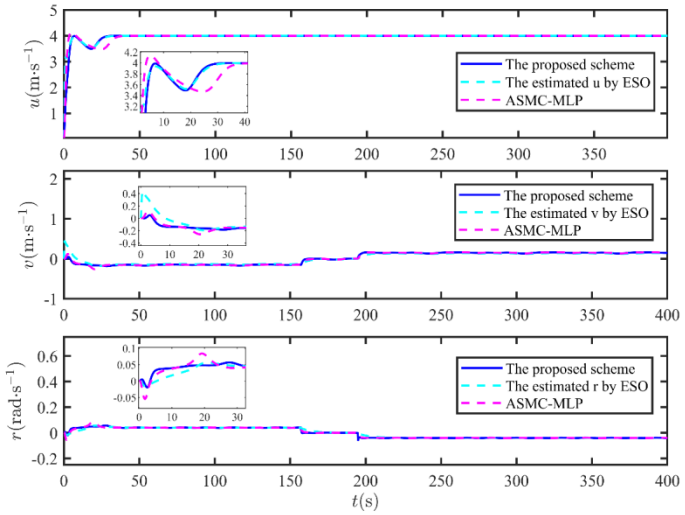

Fig. 8. The comparison of actual and estimated velocities in the proposed scheme and ASMC-MLP.

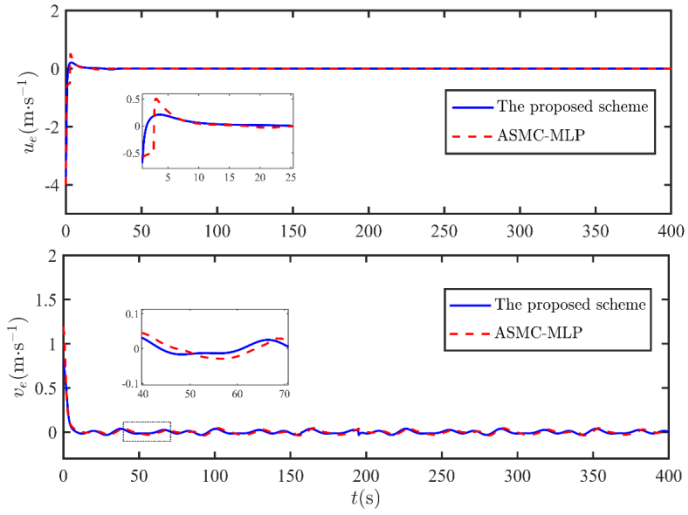

Fig. 9. The curves of velocity tracking errors.

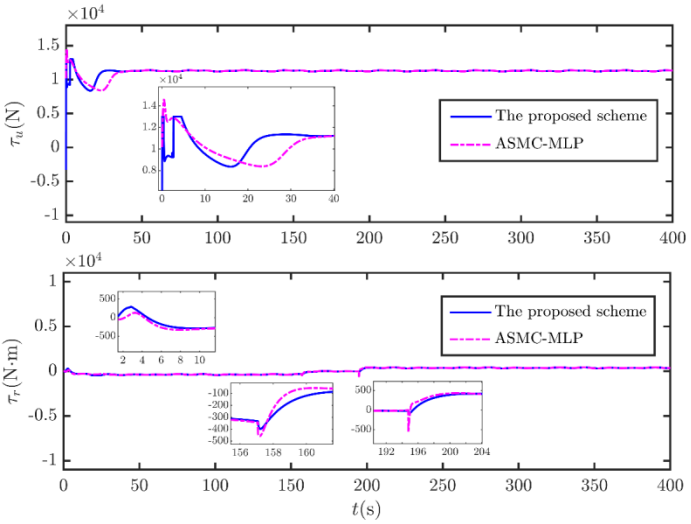

Fig. 10. The comparison curves of control inputs.

The control inputs τ_u and τ_r are presented in Fig. 10.It can be observed that the control inputs of the proposed scheme have reached saturation at the beginning, while the control inputs of the comparative schemehave large peaks and exceed the maximum range that the actuator can provide. Therefore, the results in Figure 10prove that the proposed controller can still make the system run stably even under input saturation and have better control performance. Furthermore,the unmeasurable velocitiesof the USV are estimated by the ESO and the correspondingestimate error is shown inFig. 11,where the velocity estimation errors could converge eventually to a small neighborhoodnear the origin.Fig. 12shows the estimation of lumped disturbances by the ESO.Therefore, it is revealed that the designed ESO can observe and estimate unmeasurable velocitiesand lumped disturbances with tiny errors, and has an excellentestimationperformance. Fig. 13shows that the adaptive law can estimate the upper bound of the external disturbance by choosing the appropriate parameters. As can be seen in Fig. 14, the model uncertainties of the USV can be estimated and approximated accurately by employing the MLP neural network. According to the above simulation results, we can conclude that the proposed controller has faster convergence and better robustnessperformance.

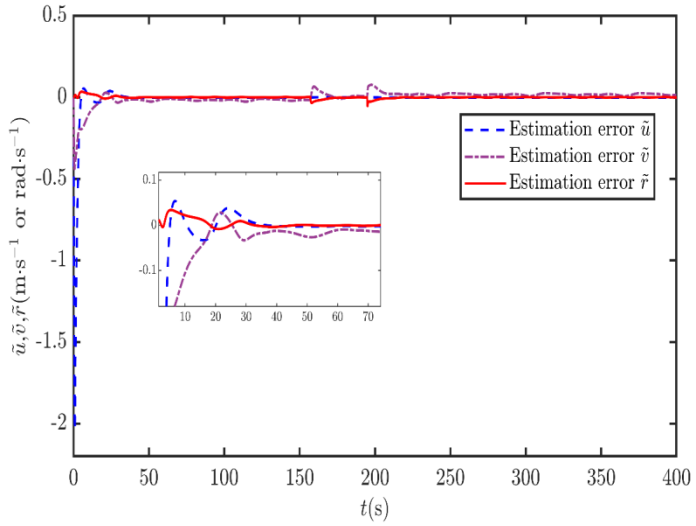

Fig. 11. The velocity estimation errors of ESO.

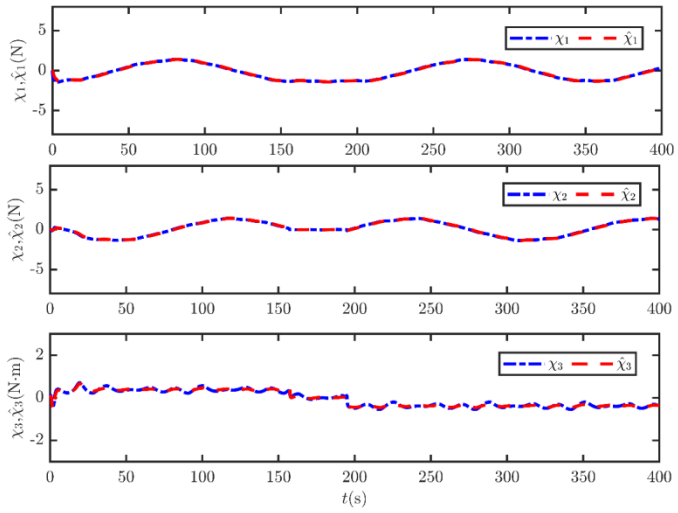

Fig. 12. The lumped disturbances and observer estimations.

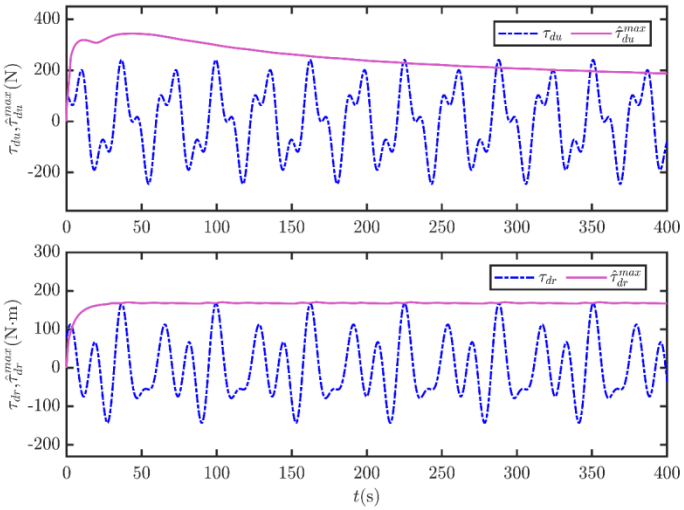

Fig. 13. The external disturbances and their boundary estimations.

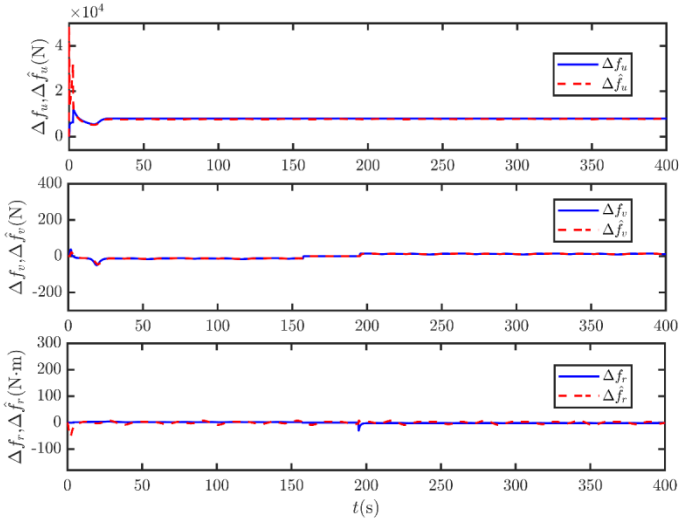

Fig. 14. The model uncertainties curves approximated by MLP.

5. Conclusions

This paper has proposed anNTSMC schemefor trajectory tracking control of the underactuated USV based on the nonlinear mathematical model subject to model uncertainties and external disturbances.The scheme is presented bycombing a nonlinear ESO,neural shunt model, andMLP neural network with adaptive technology. To address the problem that the velocity is difficult to measure in practice, a nonlinear ESO is designed in this paper, which can accurately estimate the unmeasurable velocitiesand lumped disturbances. To enhance the control system robustness, the MLP-based RBF neural network is adopted to approximateand compensate for the model uncertainties. Meanwhile, the adaptive law is designed to compensate for neural network approximation errors and disturbances. Moreover, the neural shunt model is employed to solve the differential explosion problem of virtual control quantity.Furthermore, the overallstability of the closed-loop control system is strictly guaranteed by Lyapunov theory,and the tracking errors are proved to converge to a small neighborhood of the origin. Finally, comparative numerical simulationsare carried out and the MIAE indexes are calculated simultaneously to analyze the tracking performance.The simulation resultsintensively demonstrate the effectiveness and superiority of the proposed scheme.

In the future, we willconsider the dynamiccharacteristics of the propulsor and quantitatively analyze how much computational burden can be reduced,and the designed controllerwill be applied for practical experiments.

Declaration of competing interest

The authors declare that they do not have any commercial interests or personal relationships that could have appeared to influence the work reported in this paper.

Acknowledgments

This work was supported by the National Natural Science Foundation of China (52271322).The authors would like to thank anonymous reviewers for their valuable comments to improve the quality of this article.

References

Chen, D., Zhang, J., Li, Z., 2022. A Novel Fixed-Time Trajectory Tracking Strategy of Unmanned Surface Vessel Based on the Fractional Sliding Mode Control Method. Electronics 11 (5).

Chen, X., Liu, Z., Zhang, J., Zhou, D., Dong, J., 2018. Adaptive sliding-mode path following control system of the underactuated USV under the influence of ocean currents. Journal of Systems Engineering and Electronics 29 (6), 1271-1283.

Chen, Z., Zhang, Y., Nie, Y., Tang, J., Zhu, S., 2020. Adaptive Sliding Mode Control Design for Nonlinear Unmanned Surface Vessel Using RBFNN and Disturbance-Observer. Ieee Access 8, 45457-45467.

Chen, Z., Zhang, Y.G., Zhang, Y.M., Nie, Y., Tang, J.Z., Zhu, S.Q., 2019. Disturbance-

Observer-Based Sliding Mode Control Design for Nonlinear Unmanned Surface Vessel With Uncertainties. Ieee Access 7, 148522-148530.

Deng, Y.J., Zhang, X.K., Im, N., Zhang, G.Q., Zhang, Q., 2020. Model-Based Event-Triggered Tracking Control of Underactuated Surface Vessels With Minimum Learning Parameters. Ieee Transactions on Neural Networks and Learning Systems 31 (10), 4001-4014.

Gonzalez-Garcia, A., Castaeda, H., 2021. Adaptive Integral Terminal Sliding Mode Control for an Unmanned Surface Vehicle Against External Disturbances.

Jiang, K.Y., Mao, L., Su, Y.M., Zheng, Y.X., 2021. Trajectory Tracking Control for Underactuated USV with Prescribed Performance and Input Quantization. SYMMETRY-BASEL 13 (11).

Jiang, Q., Li, Y., Liao, Y., Miao, Y., Jiang, W., Wu, H., 2019. Information fusion model-free adaptive control algorithm and unmanned surface vehicle heading control. Applied Ocean Research 90.

Lin, M., Zhang, Z., Pang, Y., Lin, H., Ji, Q., 2022. Underactuated USV path following mechanism based on the cascade method. Sci Rep 12 (1), 1461.

Liu, Z., Zhang, Y., Yu, X., Yuan, C., 2016. Unmanned surface vehicles: An overview of developments and challenges. Annual Reviews in Control 41, 71-93.

Lu, Y., A, G.Z., Sun, Z., Zhang, W., 2018. Adaptive cooperative formation control of autonomous surface vessels with uncertain dynamics and external disturbances. Ocean Engineering 167, 36-44.

Martinsen, A.B., Lekkas, A.M., Gros, S., 2022. Reinforcement learning-based NMPC for tracking control of ASVs: Theory and experiments. Control Engineering Practice 120.

Mu, D.D., Wang, G.F., Fan, Y.S., 2017. Design of Adaptive Neural Tracking Controller for Pod Propulsion Unmanned Vessel Subject to Unknown Dynamics. Journal of Electrical Engineering & Technology 12 (6), 2365-2377.

Mu, D.D., Wang, G.F., Fan, Y.S., Qiu, B.B., Sun, X.J., 2018. Adaptive Trajectory Tracking Control for Underactuated Unmanned Surface Vehicle Subject to Unknown Dynamics and Time-Varing Disturbances. Applied Sciences-Basel 8 (4).

Pan, C.-Z., Lai, X.-Z., Yang, S.X., Wu, M., 2015. A biologically inspired approach to tracking control of underactuated surface vessels subject to unknown dynamics. Expert Systems with Applications 42 (4), 2153-2161.

Piao, Z.J., Guo, C., Sun, S., 2020. Adaptive Backstepping Sliding Mode Dynamic Positioning System for Pod Driven Unmanned Surface Vessel Based on Cerebellar Model Articulation Controller. Ieee Access 8, 48314-48324.

Qin, H., Li, C., Sun, Y., 2019. Adaptive neural network‐based fault‐tolerant trajectory‐tracking control of unmanned surface vessels with input saturation and error

constraints. Iet Intelligent Transport Systems 14 (5), 356-363.

Qiu, B., Wang, G., Fan, Y., Mu, D., Sun, X., 2019. Adaptive Sliding Mode Trajectory Tracking Control for Unmanned Surface Vehicle with Modeling Uncertainties and Input Saturation. Applied Sciences-Basel 9 (6).

Rangel, M.A.G., Manzanilla, A., Suarez, A.E.Z., Munoz, F., Salazar, S., Lozano, R., 2020. Adaptive Non-singular Terminal Sliding Mode Control for an Unmanned Underwater Vehicle: Real-time Experiments. International Journal of Control Automation and Systems 18 (3), 615-628.

Shen, Z., Bi, Y., Wang, Y., Guo, C., 2020a. MLP neural network-based recursive sliding mode dynamic surface control for trajectory tracking of fully actuated surface vessel subject to unknown dynamics and input saturation. Neurocomputing 377, 103-112.

Shen, Z., Wang, Q., Dong, S., Yu, H., 2022. Dynamic surface control for tracking of unmanned surface vessel with prescribed performance and asymmetric time-varying full state constraints. Ocean Engineering 253, 111319.

Shen, Z., Wang, Y., Yu, H., Guo, C., 2020b. Finite-time adaptive tracking control of marine vehicles with complex unknowns and input saturation. Ocean Engineering 198.

Sun, X., Wang, G., Fan, Y., 2019. Model Identification and Trajectory Tracking Control for Vector Propulsion Unmanned Surface Vehicles. Electronics 9 (1).

Sun, Z., Sun, H., Li, P., Zou, J., 2022. Formation Control of Multiple Underactuated Surface Vessels with a Disturbance Observer. Journal of Marine Science and Engineering 10 (8), 12.

Van, M., 2019. An enhanced tracking control of marine surface vessels based on adaptive integral sliding mode control and disturbance observer. ISA Trans 90, 30-40.

Wan, L.L., Su, Y.X., Zhang, H.J., Tang, Y.C., Shi, B.H., 2018. Neural adaptive sliding mode controller for unmanned surface vehicle steering system. Advances in Mechanical Engineering 10 (9).

Wang, N., Zhu, Z., Qin, H., Deng, Z., Sun, Y., 2021. Finite-time extended state observer-based exact tracking control of an unmanned surface vehicle. International Journal of Robust and Nonlinear Control 31 (5), 1704-1719.

Wang, Q., Wei, J., Li, C., Zhu, H., Yang, J., 2018. Attitude Control for Spacecraft with MSGMW based on Sliding Mode Controller and Extended State Observer. IEEE.

Yao, Q., 2022. Fixed-time trajectory tracking control for unmanned surface vessels in the presence of model uncertainties and external disturbances. International Journal of Control 95 (5), 1133-1143.

Yu, Y., Guo, C., Yu, H., 2019. Finite-Time PLOS-Based Integral Sliding-Mode Adaptive Neural Path Following for Unmanned Surface Vessels With Unknown Dynamics and Disturbances. IEEE Transactions on Automation Science and Engineering 16 (4), 1500-1511.

Zhang, G.Q., Chu, S.J., Huang, J.S., Zhang, W.D., 2022. Robust adaptive fault-tolerant control for unmanned surface vehicle via the multiplied event-triggered mechanism. Ocean Engineering 249.

Zhang, C., Wang, C., Wei, Y., Wang, J., 2020. Neural-Based Command Filtered Backstepping Control for Trajectory Tracking of Underactuated Autonomous Surface Vehicles. Ieee Access 8, 42481-42490.

Zhang, J., Yu, S., Yan, Y., 2019. Fixed-time extended state observer-based trajectory tracking and point stabilization control for marine surface vessels with uncertainties and disturbances. Ocean Engineering 186, 106109.

Zhao, Y., Sun, X., Wang, G., Fan, Y., 2021. Adaptive Backstepping Sliding Mode Tracking Control for Underactuated Unmanned Surface Vehicle With Disturbances and Input Saturation. Ieee Access 9, 1304-1312.

Zheng, Z., Zou, Y., 2016. Adaptive integral LOS path following for an unmanned airship with uncertainties based on robust RBFNN backstepping. ISA Trans 65, 210-219.

Zhou, C., Gu, S., Wen, Y., Du, Z., Xiao, C., Huang, L., Zhu, M., 2020. The review unmanned surface vehicle path planning: Based on multi-modality constraint. Ocean Engineering 200, 107043.

Zhu, G., Du, J., 2020. Global Robust Adaptive Trajectory Tracking Control for Surface Ships Under Input Saturation. Ieee Journal of Oceanic Engineering 45 (2), 442-450.